Tuning intermolecular interactions with nanostructured environments

Mausumi Chattopadhyaya,[†] Jan Hermann,[†] Igor Poltavsky,[‡] and Alexandre Tkatchenko[*,‡,†]

†*Fritz-Haber-Institut der Max-Planck-Gesellschaft, Faradayweg 4–6, 14195 Berlin, Germany*

‡*Physics and Materials Science Research Unit, University of Luxembourg, L-1511 Luxembourg*

E-mail: alexandre.tkatchenko@uni.lu

Abstract

It is known that interactions between molecules may change in the presence of nanostructures. However, the exact mechanisms that dictate the tuning of intermolecular interactions remain largely unexplored in computational studies. Here, we employ density-functional calculations with the recently developed many-body dispersion (MBD) method to investigate intermolecular three-body interaction energies (where bodies can be molecules or nanostructures) in a set of nanocomposites. We analyze three representative complexes that display distinct behavior in their interaction profiles, and unravel the physical reasons behind the observed differences. We demonstrate that many-body vdW interactions can be repulsive, attractive, or neutral with respect to a pairwise treatment of vdW dispersion interactions. Our results indicate that vdW interactions in a given complex can be tuned by suitably choosing its environment. Such tuning may lead either to stabilization or destabilization of the complex, establishing many-body interactions as a useful mechanism for designing novel nanomaterials with desired properties.

Introduction

The theory of non-covalent interactions and especially of van der Waals (vdW) dispersion interactions[1,2] provides the necessary tools for description of novel nanotechnological processes such as self-assembly, molecular recognition, or template-directed synthesis.[3] Dimensionality, mutual orientation, and alignment of nanometer-sized structural motifs have come to play a central role in the understanding of physical and chemical mechanisms that determine properties of nanostructured materials.[4] The ease of designing and crafting new structural patterns opened the possibility of tuning molecular processes by choosing an appropriate nanostructured environment. But such engineering requires an understanding of how intermolecular interactions are influenced by the presence of other bodies in the environment—a topic that is understood far less than the interactions of isolated complexes in the gas phase.

Low-dimensional carbon-based structures—graphene sheets, carbon nanotubes (CNTs), and fullerenes—belong to the most studied classes of nanostructured materials. In particular, their composites with smaller organic molecules attract attention due to their unique mechanical, chemical, and electronic properties.[3–17] For instance, the electronic structure of graphene, already extraordinary in an isolated

sheet, can be further tuned by the presence of an adsorbed molecule;[18,19] protein molecules can be trapped inside biosensors based on CNTs by utilizing the strong interactions in π–π stacked systems.[20–22] Despite numerous studies, however, solid theoretical understanding of the role of vdW interactions in nanocomposite materials is still missing, in part due to their challenging many-body nature, which is especially manifesting in low-dimensional systems.[23–25]

The majority of state-of-the-art methods for predicting material properties are based on density functional theory (DFT). The indisputable importance of vdW interactions in modern material science combined with the notorious lack of them in popular density functionals led to development of many approaches that incorporate dispersion into DFT.[26–31] Among them, perhaps the most popular class of methods is based on a sum over atom pairs of the asymptotic C_6/R^6 term damped at short distances.[32–36] But despite many successful predictions, these methods can fail qualitatively and quantitatively.[24,37–40] Most of these failures arise from neglecting the collective nature of the electrodynamic response in the pairwise approximation. But in fact, the electrodynamic response can play an important role in a wide range of nanomaterials because it scales nontrivially with system size and depends heavily on their dimensionality.[41–44]

A straightforward improvement over the pairwise methods is to extend the sum over atom pairs to a sum over atom pairs *and* triples—the latter is the so-called Axilrod–Teller–Muto (ATM) term C_9/R^9—which has been recently incorporated into several approximate vdW methods.[45,46] The contribution of the ATM term to the binding energy can range from single-digit percents, which is typical, to 10–20% for systems such as the adenine–thymine complex, to 50% in exceptional cases such as the graphene bilayer.[47] The ATM correction somewhat extends the applicability of pairwise methods, but eventually fails for many systems as well, because the still higher-order correlation energy terms—the result of the full electrodynamic screening—are missing. In contrast, the recently developed many-body dispersion (MBD) method[48,49] considers all orders of the correlation energy by mapping the atomic electrodynamic response to quantum harmonic oscillators and then solving the corresponding Hamiltonian in an exact numerical way. As a result, MBD can accurately describe complex systems bound by vdW interactions. For instance, it reproduces nontrivial modifications of the power laws of vdW interaction energy in low-dimensional nanostructures,[50] or nontrivial scaling of the electrodynamic response of carbon-based nanomaterials.[41] Both of these effects are completely absent in pairwise as well as ATM-corrected methods.

In this work, we apply the infinite-order MBD method, pairwise Tkatchenko and Scheffler[32] (TS) method, and the density functional of Perdew, Burke, and Ernzerhof (PBE),[51] which does not describe dispersion, to answer the question of how the interaction between two molecules or nanostructures changes in the presence of a third one. We select a representative set of systems that display three different interaction energy profiles, and pay particular attention to identify the physical reasons (ingredients of the methods) that are responsible for the observed differences. Our results highlight the possibility of designing nanomaterials that, as hosts, could tune interactions of guest molecular systems.

Methods

The total energy of an arbitrary 3-body system (in this work, bodies refer to molecules or nanostructures), E_{A+B+C}, can be represented as

$$E_{A+B+C} = \sum_{\alpha} E_{\alpha} + \sum_{\alpha,\beta} E^{(2)}_{\alpha\beta} + E^{(3)}, \qquad (1)$$

where E_α ($\alpha \in A, B, C$) are total energies of the isolated subsystems, $E^{(2)}_{\alpha\beta} = E_{\alpha+\beta} - E_\alpha - E_\beta$ are the 2-body interaction energies, and $E^{(3)}$ is the 3-body interaction energy term. $E^{(3)}$ will be the main focus of this study, since it determines the part of the interaction energy which depends non-trivially upon the states of all three com-

ponents of a 3-body complex. Thus, $E^{(3)}$ can be considered to be a modification of the interaction between two bodies in a presence of the third body.

To reveal the role of many-body effects in 3-body interactions, we calculate $E^{(3)}$ on three different levels of theory by employing the density functional of Perdew, Burke, and Ernzerhof (PBE),[51] and in addition account for vdW interactions with the TS or MBD methods. PBE is capable of describing most electronic effects present in the systems considered here, except for the perhaps most relevant one—long-range vdW correlation. TS is an interatomic pairwise method that accounts for changes in atomic polarizabilities and C_6 coefficients due to covalent bonding via changes in the electron density. In particular, TS obtains the polarizability of the i-th atom, α_i, by scaling the reference free-atom polarizability α_i^{free} with a ratio of effective volumes of an atom in a molecule, V_i, and of a free atom, V_i^{free},

$$\frac{\alpha_i}{\alpha_i^{\text{free}}} = \frac{V_i}{V_i^{\text{free}}} = \frac{\int w_i(\mathbf{r}) n(\mathbf{r}) r^3 \mathrm{d}\mathbf{r}}{\int n_i^{\text{free}}(\mathbf{r}) r^3 \mathrm{d}\mathbf{r}}, \qquad (2)$$

where n is the total electron density, n_i^{free} is the electron density of a free atom, and w_i is the Hirshfeld weight defined as

$$w_i = \frac{n_i^{\text{free}}(\mathbf{r})}{\sum_j n_j^{\text{free}}(\mathbf{r})}. \qquad (3)$$

The atomic polarizabilities obtained in this way (C_6 coefficients are treated similarly) are then used in the standard pairwise sum to obtain the long-range correlation energy (see Ref.[32] for details).

MBD also uses fragmentation of a system to atoms, but the subsequent treatment of the atomic response functions goes beyond the pairwise approximation and accounts for higher-order electron correlation terms up to infinite order in dipole coupling. Specifically, MBD starts with TS atomic dipole polarizabilities, but further screens them using a self-consistent dipole equation,

$$\boldsymbol{\alpha}^{\text{MBD}} = \boldsymbol{\alpha}^{\text{TS}} - \boldsymbol{\alpha}^{\text{TS}} \mathbf{T}_{\text{sr}} \boldsymbol{\alpha}^{\text{MBD}}, \qquad (4)$$

where $\mathbf{T}_{\text{sr}}$ is a short-range part of the dipole potential. Solving the Hamiltonian for quantum harmonic oscillators parametrized with these screened polarizabilities then provides the MBD long-range correlation energy,

$$E_{\text{c}}^{\text{MBD}} = -\frac{1}{2\pi} \int_0^\infty \mathrm{d}u \sum_{n=2}^{\infty} \frac{1}{n} \operatorname{Tr}\left[\left(\boldsymbol{\alpha}^{\text{MBD}} \mathbf{T}_{\text{lr}}\right)^n\right], \qquad (5)$$

where $\mathbf{T}_{\text{lr}}$ is the long-range part of the dipole potential (see Refs.[48,49] for details).

All calculations were performed with the FHI-aims all-electron code[52] using the standard "tight" basis set and grid settings.

Results

We employ three methods in this work, of which PBE+MBD is the most general, while PBE+TS and bare PBE can be considered approximations to it. Comparison between the three enables us to understand the influence of many-body effects on intermolecular interactions. To verify the performance of the methods for the class of carbon-based nanocomposites, we calculated the binding energy of a benzene molecule and a single graphene sheet. The obtained values of $E^{(2)}$ with PBE, PBE+TS, and PBE+MBD at equilibrium distances are -0.7 kcal/mol (4.1 Å), -13.1 kcal/mol (3.4 Å), and -9.0 kcal/mol (3.4 Å), respectively. The experimental adsorption enthalpy for this system is -12 ± 2 kcal/mol,[5] placing the PBE+TS prediction well within and PBE+MBD slightly below the experimental uncertainty. Employing a more accurate hybrid functional instead of PBE would make binding stronger, bringing MBD results closer to experiment.[53] Furthermore, experimental measurements are carried out at finite temperature, while the calculations are done at 0 K. Taking this difference into account, both PBE+TS and PBE+MBD yield results in fair agreement with experiment. Nevertheless, already this application, in particular the difference between TS and MBD, shows that higher-order correlation terms (present in MBD, neglected in TS) can result in a significant contribution to the binding energy of molecules to nanostructures. In

contrast, the employment of the bare PBE functional leads to severe underestimation of the binding energy and incorrect adsorption height. This demonstrates the importance of long-range electron correlations for an accurate description of carbon-based nanocomposites.

Advancing from two- to three-body systems, we studied three representative cases (see Figure 1a): (i) two pyrene molecules (PY) and a single sheet of graphene (GR) between them, labelled PY–GR–PY, (ii) two carbon zigzag (7,0) nanotubes separated by a fullerene C_{60} molecule, labelled CNT–C_{60}–CNT, and (iii) two pyrene molecules and a phosphorene layer (P) between them, labelled as PY–P–PY. The systems are modelled using periodic boundary conditions (PBC) with unit cell dimensions reported in Table 1, and we verified that interactions between ghost periodic images of the molecules and layers are negligible.

The binding energies at equilibrium geometry of the respective two-body subsystems are 21.9, 10.3, and 18.6 kcal/mol (950, 450, and 810 meV) for graphene–pyrene, CNT–C_{60}, and phosphorene–pyrene, respectively. The 3-body interaction energies of the full 3-body systems that we report and analyse below are approximately by an order of magnitude smaller than these 2-body binding energies, and so could be perceived as small contributions. Nevertheless, we argue that the 3-body energies are of primary importance. The first reason is that nanostructured composites are often condensed in bulk phases, in which the importance of many-body effects increases dramatically.[50] The 2-body binding energies are expected to govern the basic structural motifs, but often cannot distinguish between different types of crystal packings (polymorphs) or higher-order structures in general. Perhaps the simplest example of this phenomenon is the structure of noble gas crystals, where simple pair potentials barely distinguish between the *hcp* and *fcc* packings, and erroneously predict the *fcc* structure to be the most stable one, while experiment unambiguously determines the *hcp* crystal structure as the global minimum at low temperature. The correct prediction for noble gas crystals is obtained only upon inclusion of the three-atom (and higher-order) vdW potentials. The second reason is that the sheer size of the nanoscale objects results in the 3-body interaction energies being comparable to or larger than the energy of thermal fluctuations, which makes our conclusions reached by studying the 3-body energies relevant to a broad set of potential applications.

Figure 1b shows three distinct patterns in the 3-body interaction energy profiles—that is, relative relationships between the three methods. As expected, in all three systems and with all three methods, the 3-body energy increases exponentially to positive values at short distances due to Pauli repulsion of the third body, which influences the electronic structure of the other two interacting bodies. But all three systems behave differently at intermediate distances. In PY–GR–PY, $E^{(3)}$ becomes significantly larger when going from the PBE level of theory to the PBE+TS description, but PBE+MBD brings it back to the PBE levels. In other words, the presence of the graphene sheet increases the attraction between two pyrene molecules significantly more when described by the PBE+TS method compared to the PBE and PBE+MBD methods. In CNT–C_{60}–CNT, the 3-body interaction energy is relatively small in the PBE and PBE+TS descriptions, but it is enhanced when going to the MBD method. Finally, in PY–P–PY, all three methods provide comparable predictions of $E^{(3)}$. The different behaviour of the methods in the three systems can be understood by analysing the various effects that are gradually accounted for as one goes from the PBE to PBE+TS to PBE+MBD levels of theory.

The binding in the three systems considered here comes mostly from vdW correlation. As such, the bare PBE functional serves as a baseline that correctly describes the Pauli repulsion, electrostatic and induction interactions, as well as the short-range part of the correlation. The TS method accounts for the long-range correlation in a pairwise manner, while deriving the atomic polarizabilities and C_6 coefficients from the electron density. Since the pairwise sum over atoms on its own results in a zero 3-body energy by definition, the contribution

Table 1: Details of calculations.

complex	lattice	parameters [Å]	k-point grid
PY–GR–PY	hexagonal	$a = 24.56$, $c = 1000$	$4 \times 4 \times 1$
CNT–C_{60}–CNT	tetragonal	$a = 400$, $c = 17.05$	$1 \times 1 \times 10$
PY–P–PY	orthorombic	$a = 26.51$, $b = 35.01$, $c = 1000$	$4 \times 4 \times 1$

to $E^{(3)}$ from TS comes entirely from the short-range many-body effects in the electron density caused by the presence of the third body, that subsequently manifest in small changes in the polarizabilities and C_6 coefficients. The MBD model is based on the atomic parametrization of the TS method, but the subsequent treatment via the quantum-mechanical dipole-coupled Hamiltonian leads to two additional effects that contribute to the 3-body energy. First, the screening of atomic polarizabilities leads to an improved description of the short-range many-body effects beyond those captured in the slight changes in the electron density. Second, the MBD model accounts consistently for all orders of the correlation of the density fluctuations, leading to long-range many-body effects in the correlation energy beyond the pairwise description in TS. In the following paragraphs, we analyze the contributions of these three distinct effects—(i) the short-range effects captured in changes in the electron density, (ii) the short-range effects beyond those, and (iii) the long-range effects originating from higher orders of the electron correlation—to the 3-body interaction energy.

In an atomic pairwise method, such as TS, the only contribution to the 3-body interaction energy comes from changes of the polarizabilities due to the presence of the third body. In our case, these changes have two sources: first, the change of the polarizability of the middle sandwiched system (GR, C_{60}, or P) due to the presence of the second outer body (PY or CNT) with respect to the case with only a single outer body; second, the change of the polarizability of the outer body due to the presence of the middle body. Figure 1c presents the change in the TS polarizability of the sandwiched system in all three complexes along a dissociation path due to the presence of either one or two outer interacting bodies. The change is caused by the valence electron density of the system slightly shifting either towards or away from the intermolecular region, depending on the electronic structure of the interacting bodies. This shift subsequently either increases or decreases the effective atomic volumes (see Eq. 2), leading to a corresponding change in polarizabilities. This short-range many-body effect is described by the TS method through its dependence on the electron density, whereas it would be neglected altogether by methods that model the atomic polarizabilities based purely on geometrical considerations, such as the DFT-D3 method.[45] In all three complexes, the presence of the two outer bodies leads to an approximately twofold change in the polarizability compared to a single body (Fig. 1c), demonstrating a linear regime of this density perturbation. Of the three complexes, the effect is largest for PY–GR–PY where the polarizability is increased, explaining the substantial negative (binding) contribution of the TS method to $E^{(3)}$ with respect to bare PBE for this complex. The other contribution to $E^{(3)}$—due to the change in the polarizability of the pyrene molecules in the presence of the graphene sheet—is negligible, since the 2-body interaction energies of the outer bodies are small compared to those of the outer and middle body.

In the MBD method, the atomic density fluctuations are correlated in a collective manner, in contrast to the pair-by-pair correlations in TS. Due to the coupling to an underlying density functional, this correlation is range-separated, leading to two distinct mechanisms that contribute to the 3-body interaction energy on top of that already present in TS, as explained above. Figure 1d presents the short-range effect of these two, namely the screening of the atomic polarizabilities, which

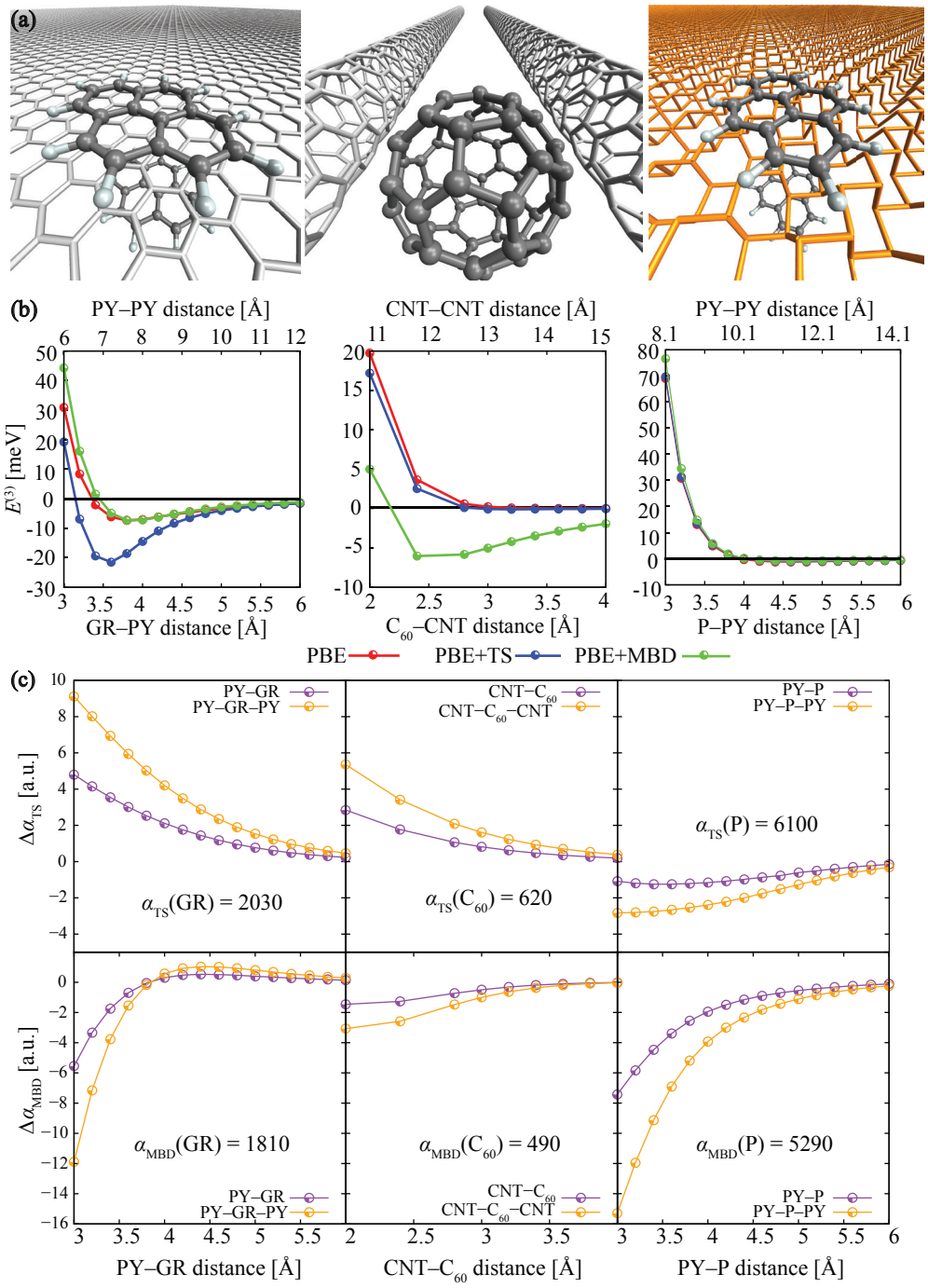

Figure 1: **Three-body interaction energies and polarizabilities of three nanocomposites.** (**a**) 3D illustrations of the structures. From left to right: PY–GR–PY, CNT–C_{60}–CNT, and PY–P–PY. (**b**) Three-body interaction energies along dissociation paths. In all cases, the outer bodies are moved away from the middle body in a symmetric fashion. The reported distances on the bottom and upper x-axis are minimum distances between convex envelopes of the objects (surface-to-surface). Thus, the distance between the outer bodies is double the distance to the middle body plus its width, which is 0, 7.0, and 2.1 Å for graphene, C_{60}, and phosphorene, respectively. (**c**) Change in the TS (top) and MBD (bottom) projected polarizabilities of the middle body due to interaction with one (violet) and two (yellow) outer bodies.

is applied on top of the hybridization effects in the electron density captured by TS. In the two carbon-based complexes (PY–GR–PY and CNT–C_{60}–CNT), the screening shifts the polar-

Table 2: Three-body interaction energies [meV] computed with different methods.

complex	distance [Å]	$E^{(3)}_{\mathrm{PBE}}$	$E^{(3)}_{\mathrm{PBE+TS}}$	$E^{(3)}_{\mathrm{PBE+MBD(2)}}$	$E^{(3)}_{\mathrm{PBE+MBD}}$
PY–GR–PY	3.4	−2.1	−19.4	1.9	1.5
CNT–C_{60}–CNT	2.4	3.7	2.5	3.0	-6.0
PY–P–PY	4.0	−0.4	0.1	−1.0	0.5

izabilities in the opposite direction than the TS hybridization (Figure 1c), whereas in the phosphorene complex, the two effects are additive. We attribute it to the different structures of the graphene and phosphorene layers, leading to different geometrical patterns in the alignment of the fluctuating atomic dipoles. In particular, the purely planar structure of graphene discourages fluctuations in the out-of-plane direction, whereas the two layers of phosphorus atoms in a single phosphorene sheet and the covalent bonds between them easily allow for such fluctuations. The contribution of the other distinct feature of the MBD method—the higher-order correlation terms—can be analysed by comparing the full MBD energy to only the second-order term, denoted MBD(2), which corresponds to $n = 2$ in Eq. 5. The data in Table 2 reveal that this effect is dominant in the fullerene complex, whereas it is relatively small in the other two complexes. We explain this difference by CNTs being infinitely extended in one dimension, in contrast to the pyrene molecules, which are zero-dimensional.

Further expanding the range of investigated materials, we found that $E^{(3)}$ in the boron nitride (BN), molybdenum sulphide (MoS_2) and benzene (BZ) analogues of PY–P–PY (P replaced with BN or MoS_2, PY replaced with BZ, and combinations thereof) behaves qualitatively in the same way (see SI for details).

Theoretical guidance of practical material design is best achieved with qualitative rules like scaling laws. As an example of such a law, the 3-body interaction energy of a series of increasingly large fullerene dimers separated by a single graphene sheet scales non-linearly with system size (Fig. 2). Fitting a power-law function, ax^b, to the data gives an approximate formula

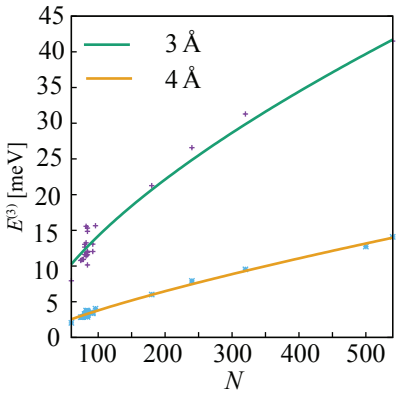

Figure 2: Three-body interaction energy (using MBD) of two spherical fullerenes C_N sandwiching a graphene sheet, which is at distance of 3 Å (green) and 4 Å (yellow) from the fullerenes. A constant Hirshfeld volume of 0.845 was used for all carbon atoms. Full data are available in Tables S1 and S2 in the SI.

for the scaling,

$$E^{(3)}(\mathrm{C}_N\text{–GR–C}_N) \sim N^{0.67} \doteq N^{\frac{2}{3}} \qquad (6)$$

where N is the number of atoms in the fullerene molecule. We currently work on simplest possible analytical models that would be capable of explaining this dependence.

Conclusions

The tendency of modern material science towards nanoscale combined with the increasing importance of computational results in material design motivates the rapid development of vdW methods for DFT. The primary focus used to be the description of isolated complexes bound by vdW interactions. However, as more general and accurate methods for this *in vacuo* problem appear, the more the influence of material environment comes to the forefront.

In this work, we have demonstrated that a correct description of environmental effects within fragment-based vdW methods requires proper accounting for both short-range (electron density changes, short-range screening of polarizability) and long-range (higher-order energy terms) contributions. In particular, the relative magnitude of these effects rapidly changes across different nanocomposite materials. This finding has two major consequences. First, the neglect of subtle electronic effects in vdW interactions is even less justifiable for 3-body energies than for 2-body energies, and hence for predictions of environmental effects. Despite our results being only preliminary and requiring future studies to achieve deeper understanding of the role of many-body intermolecular interactions in nanoscale materials, it nevertheless becomes obvious that the development of vdW methods should target the accuracy for not only 2-body but for higher-body interactions as well. Second, the influence of material environments on noncovalent interactions is selective and specific rather than generic. This opens the possibility to tune vdW interactions in a given complex by suitably choosing the environment.

Acknowledgement We acknowledge the financial support of the Alexander von Humboldt Foundation, the European Research Council (ERC-StG VDW-CMAT), and the DFG Research Network (SFB-951).

Supporting Information Available

The following files are available free of charge. Three-body interaction energies of: analogues of PY–P–PY with P replaced with boron nitride or molybdenum sulphide, PY replaced with a benzene molecule, and combinations thereof; dimers of fullerenes from a series of an increasing size separated by a graphene sheet.

References

(1) Langbein, D. *Springer Tracts in Modern Physics*; Springer Berlin Heidelberg, 1974; pp 1–139.

(2) Parsegian, V. A. *Van der Waals forces: a handbook for biologists, chemists, engineers, and physicists*; Cambridge University Press, 2005.

(3) Dai, H. Carbon nanotubes: synthesis, integration, and properties. **2002**, *35*, 1035–1044.

(4) Yu, M.-F.; Files, B. S.; Arepalli, S.; Ruoff, R. S. Tensile loading of ropes of single wall carbon nanotubes and their mechanical properties. **2000**, *84*, 5552.

(5) Zacharia, R.; Ulbricht, H.; Hertel, T. Interlayer cohesive energy of graphite from thermal desorption of polyaromatic hydrocarbons. **2004**, *69*, 155406.

(6) Chakarova-Käck, S. D.; Schröder, E.; Lundqvist, B. I.; Langreth, D. C. Application of van der Waals density functional to an extended system: Adsorption of benzene and naphthalene on graphite. **2006**, *96*, 146107.

(7) Antony, J.; Grimme, S. Structures and interaction energies of stacked graphene–nucleobase complexes. **2008**, *10*, 2722–2729.

(8) Rochefort, A.; Wuest, J. D. Interaction of substituted aromatic compounds with graphene. **2008**, *25*, 210–215.

(9) Podeszwa, R. Interactions of graphene sheets deduced from properties of polycyclic aromatic hydrocarbons. **2010**, *132*, 044704.

(10) Wuest, J. D.; Rochefort, A. Strong adsorption of aminotriazines on graphene. **2010**, *46*, 2923–2925.

(11) Bradley, K.; Gabriel, J.-C. P.; Star, A.; Grüner, G. Short-channel effects in

contact-passivated nanotube chemical sensors. **2003**, *83*, 3821–3823.

(12) Zhang, M.; Atkinson, K. R.; Baughman, R. H. Multifunctional carbon nanotube yarns by downsizing an ancient technology. **2004**, *306*, 1358–1361.

(13) Sotiropoulou, S.; Chaniotakis, N. A. Carbon nanotube array-based biosensor. **2003**, *375*, 103–105.

(14) Wu, Z.; Chen, Z.; Du, X.; Logan, J. M.; Sippel, J.; Nikolou, M.; Kamaras, K.; Reynolds, J. R.; Tanner, D. B.; Hebard, A. F. Transparent, conductive carbon nanotube films. **2004**, *305*, 1273–1276.

(15) Fan, S.; Chapline, M. G.; Franklin, N. R.; Tombler, T. W.; Cassell, A. M.; Dai, H. Self-oriented regular arrays of carbon nanotubes and their field emission properties. **1999**, *283*, 512–514.

(16) Burt, D. P.; Wilson, N. R.; Weaver, J. M.; Dobson, P. S.; Macpherson, J. V. Nanowire probes for high resolution combined scanning electrochemical Microscopy-Atomic force Microscopy. **2005**, *5*, 639–643.

(17) Kong, J.; Franklin, N. R.; Zhou, C.; Chapline, M. G.; Peng, S.; Cho, K.; Dai, H. Nanotube molecular wires as chemical sensors. **2000**, *287*, 622–625.

(18) Chen, W.; Chen, S.; Qi, D. C.; Gao, X. Y.; Wee, A. T. S. Surface transfer p-type doping of epitaxial graphene. **2007**, *129*, 10418–10422.

(19) Zhang, Z.; Huang, H.; Yang, X.; Zang, L. Tailoring electronic properties of graphene by π–π stacking with aromatic molecules. **2011**, *2*, 2897–2905.

(20) Wang, C.-W.; Pan, C.-Y.; Wu, H.-C.; Shih, P.-Y.; Tsai, C.-C.; Liao, K.-T.; Lu, L.-L.; Hsieh, W.-H.; Chen, C.-D.; Chen, Y.-T. In Situ Detection of Chromogranin A Released from Living Neurons with a Single-Walled Carbon-Nanotube Field-Effect Transistor. **2007**, *3*, 1350–1355.

(21) Chen, R. J.; Zhang, Y.; Wang, D.; Dai, H. Noncovalent sidewall functionalization of single-walled carbon nanotubes for protein immobilization. **2001**, *123*, 3838–3839.

(22) Chen, R. J.; Bangsaruntip, S.; Drouvalakis, K. A.; Kam, N. W. S.; Shim, M.; Li, Y.; Kim, W.; Utz, P. J.; Dai, H. Noncovalent functionalization of carbon nanotubes for highly specific electronic biosensors. **2003**, *100*, 4984–4989.

(23) Tkatchenko, A. Current understanding of van der Waals effects in realistic materials. **2015**, *25*, 2054–2061.

(24) Reilly, A. M.; Tkatchenko, A. van der Waals dispersion interactions in molecular materials: beyond pairwise additivity. **2015**, *6*, 3289–3301.

(25) Dobson, J. F.; Gould, T. Calculation of dispersion energies. **2012**, *24*, 073201.

(26) Dion, M.; Rydberg, H.; Schröder, E.; Langreth, D. C.; Lundqvist, B. I. Van der Waals density functional for general geometries. **2004**, *92*, 246401.

(27) Wu, Q.; Yang, W. Empirical correction to density functional theory for van der Waals interactions. **2002**, *116*, 515–524.

(28) Grimme, S. Accurate description of van der Waals complexes by density functional theory including empirical corrections. **2004**, *25*, 1463–1473.

(29) Von Lilienfeld, O. A.; Tavernelli, I.; Rothlisberger, U.; Sebastiani, D. Optimization of effective atom centered potentials for London dispersion forces in density functional theory. **2004**, *93*, 153004.

(30) Johnson, E. R.; Becke, A. D. A post-Hartree–Fock model of intermolecular interactions. **2005**, *123*, 024101.

(31) Silvestrelli, P. L. Van der Waals interactions in DFT made easy by Wannier functions. **2008**, *100*, 053002.

(32) Tkatchenko, A.; Scheffler, M. Accurate molecular van der Waals interactions from ground-state electron density and free-atom reference data. **2009**, *102*, 073005.

(33) Kannemann, F. O.; Becke, A. D. van der Waals interactions in density-functional theory: intermolecular complexes. **2010**, *6*, 1081–1088.

(34) Steinmann, S. N.; Corminboeuf, C. Comprehensive benchmarking of a density-dependent dispersion correction. **2011**, *7*, 3567–3577.

(35) Tkatchenko, A.; Romaner, L.; Hofmann, O. T.; Zojer, E.; Ambrosch-Draxl, C.; Scheffler, M. Van der Waals interactions between organic adsorbates and at organic/inorganic interfaces. **2010**, *35*, 435–442.

(36) Marom, N.; Tkatchenko, A.; Rossi, M.; Gobre, V. V.; Hod, O.; Scheffler, M.; Kronik, L. Dispersion interactions with density-functional theory: benchmarking semiempirical and interatomic pairwise corrected density functionals. **2011**, *7*, 3944–3951.

(37) Wen, S.; Beran, G. J. Crystal Polymorphism in Oxalyl Dihydrazide: Is Empirical DFT-D Accurate Enough? **2012**, *8*, 2698–2705.

(38) Otero-De-La-Roza, A.; Johnson, E. R. A benchmark for non-covalent interactions in solids. **2012**, *137*, 054103.

(39) Marom, N.; DiStasio, R. A.; Atalla, V.; Levchenko, S.; Reilly, A. M.; Chelikowsky, J. R.; Leiserowitz, L.; Tkatchenko, A. Many-Body Dispersion Interactions in Molecular Crystal Polymorphism. **2013**, *52*, 6629–6632.

(40) Risthaus, T.; Grimme, S. Benchmarking of London dispersion-accounting density functional theory methods on very large molecular complexes. **2013**, *9*, 1580–1591.

(41) Gobre, V. V.; Tkatchenko, A. Scaling laws for van der Waals interactions in nanostructured materials. **2013**, *4*, 2341, Article.

(42) Ruzsinszky, A.; Perdew, J. P.; Tao, J.; Csonka, G. I.; Pitarke, J. M. Van der Waals coefficients for nanostructures: fullerenes defy conventional wisdom. **2012**, *109*, 233203.

(43) Dobson, J. F. Beyond pairwise additivity in London dispersion interactions. **2014**, *114*, 1157–1161.

(44) Bordag, M.; Geyer, B.; Klimchitskaya, G.; Mostepanenko, V. Lifshitz-type formulas for graphene and single-wall carbon nanotubes: van der Waals and Casimir interactions. **2006**, *74*, 205431.

(45) Grimme, S.; Antony, J.; Ehrlich, S.; Krieg, H. A consistent and accurate ab initio parametrization of density functional dispersion correction (DFT-D) for the 94 elements H-Pu. **2010**, *132*, 154104.

(46) Grimme, S. Supramolecular binding thermodynamics by dispersion-corrected density functional theory. **2012**, *18*, 9955–9964.

(47) von Lilienfeld, O. A.; Tkatchenko, A. Two-and three-body interatomic dispersion energy contributions to binding in molecules and solids. **2010**, *132*, 234109.

(48) Tkatchenko, A.; DiStasio Jr, R. A.; Car, R.; Scheffler, M. Accurate and efficient method for many-body van der Waals interactions. **2012**, *108*, 236402.

(49) Ambrosetti, A.; Reilly, A. M.; DiStasio Jr, R. A.; Tkatchenko, A. Long-range correlation energy calculated from coupled atomic response functions. **2014**, *140*, 18A508.

(50) Ambrosetti, A.; Ferri, N.; DiStasio, R. A.; Tkatchenko, A. Wavelike charge density fluctuations and van der Waals interactions at the nanoscale. **2016**, *351*, 1171–1176.

(51) Perdew, J. P.; Burke, K.; Ernzerhof, M. Generalized Gradient Approximation Made Simple. **1996**, *77*, 3865–3868.

(52) Blum, V.; Gehrke, R.; Hanke, F.; Havu, P.; Havu, V.; Ren, X.; Reuter, K.; Scheffler, M. Ab initio molecular simulations with numeric atom-centered orbitals. **2009**, *180*, 2175–2196.

(53) Liu, W.; Maaß, F.; Willenbockel, M.; Bronner, C.; Schulze, M.; Soubatch, S.; Tautz, F. S.; Tegeder, P.; Tkatchenko, A. Quantitative Prediction of Molecular Adsorption: Structure and Binding of Benzene on Coinage Metals. **2015**, *115*, 036104.

Graphical TOC Entry